Eur. Phys. J. A **11**, 47–58 (2001)

THE EUROPEAN PHYSICAL JOURNAL A

Variation of total kinetic energy and mass distributions in the fusion-fission reaction of ^{16}O, ^{19}F + ^{209}Bi at near barrier energies

L.M. Pant[a], R.K. Choudhury, A. Saxena, and D.C. Biswas

Nuclear Physics Division, Bhabha Atomic Research Centre, Mumbai 400085, India

Received: 9 April 2001 / Revised version: 10 May 2001
Communicated by D. Guerreau

Abstract. Fission fragment mass and energy distributions and their correlations have been measured for the ^{16}O and ^{19}F + ^{209}Bi reactions over a wide range of excitation energies (E^* = 30–50 MeV). It is observed that in the case of ^{16}O + ^{209}Bi reaction, the average total fragment kinetic energy, $\langle TKE \rangle$ is nearly independent of the bombarding energy. However, in the case of ^{19}F + ^{209}Bi reaction, the average total kinetic energy of the fission fragments shows a peaking behaviour near the barrier. The variation in $\langle TKE \rangle$ at near barrier energies in the ^{19}F + ^{209}Bi system seems to be correlated with corresponding strong variation in the variance of the fragment mass distribution. The present results may imply certain dynamical effects leading to compact scission configurations in the fission of ^{19}F + ^{209}Bi system at near barrier bombarding energies.

PACS. 25.70.Jj Fusion and fusion-fission reactions

1 Introduction

The mass and kinetic energy distributions of fission fragments are decided during the transition from the saddle to scission stages in the fission process, and therefore can reveal important information about the reaction mechanisms involved in the fusion-fission dynamics in the heavy-ion–induced reactions [1]. The mass distributions observed in heavy-ion–induced fission reactions are invariably of symmetric shape and single peaked, because the compound nucleus is generally formed with large excitation energy (E^*) well above the fission barrier. The fragment shell effects observed in the mass distributions in the case of light-ion–induced fission [2] are not evident in the case of heavy-ion–induced reactions, due to washing out of the shell effects at high excitation energies and angular momenta brought into the fissioning composite system by the heavy ions. In general, it is observed that the effect of increase in the excitation energy of the fissioning nucleus is on the average an increase in the width of the mass distribution. It has also been shown in earlier studies that the mass distribution of fission fragments in heavy-ion–induced fission may provide information on the reaction mechanisms involved in the fission process, due to admixture of fully equilibrated compound nuclear events and non-compound nuclear reactions such as fast fission, quasi-fission and pre-equilibrium fission etc. [3,4]. Mass distributions following such an admixture would be expected to be broader than those for normal fission, because non-compound fission reactions are expected to have more asymmetric component arising due to incomplete equilibration in mass degree of freedom. Masri *et al.* [5] reported a higher mass width for ^{40}Ar+^{165}Ho system compared to a similar composite system at nearly the same excitation energy formed through ^{20}Ne + ^{185}Re reaction, which was explained in terms of onset of fast fission in the former case. In one of our earlier measurements [6], we had carried out measurements of mass and kinetic energy distributions and angular anisotropies of the fission fragments in ^{11}B+^{237}Np and ^{16}O+^{209}Bi reaction at the bombarding energies of 76 MeV and 100 MeV, respectively. It was found that in case of ^{11}B + ^{237}Np the fragment anisotropy is independent of fragment mass, whereas in case of ^{16}O + ^{209}Bi reaction the fragment anisotropy decreases with increasing fragment mass asymmetry. This result was attributed to the different dynamical paths followed by the fragments of different mass asymmetry in the case of latter reaction. Recently, Pokrovsky *et al.* [7] observed a three component structure in the total kinetic energy distribution for ^{12}C + ^{208}Pb reaction in the range of asymmetric fission fragment masses. The mass-energy distributions of fission fragments in low excitation range for $A_{CN} > 200$ are generally explained using the concept of multimodal fission [8,9]. In a refined method of multimodal analysis applied to the experimental data in the reaction ^{18}O + ^{208}Pb, a noticeable presence of the high-energy mode S3 was found, which was attributed to the influence of the close to spherical neutron shell with $N\sim$50 in the light fission fragment [10]. Recently, the charge

[a] e-mail: lmpant@apsara.barc.ernet.in

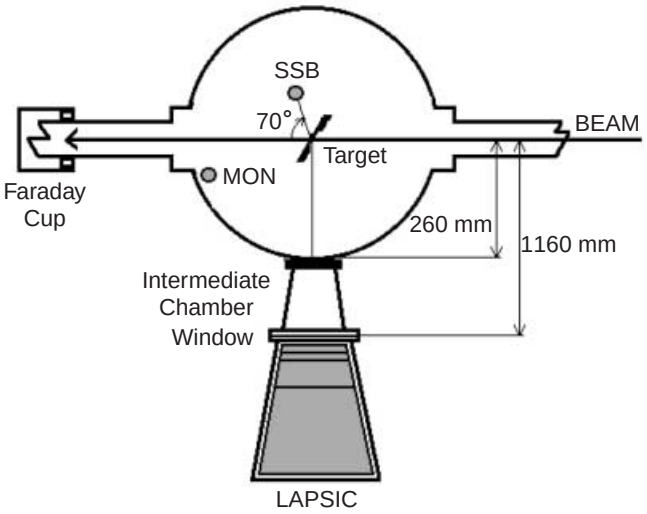

Fig. 1. Schematic diagram of the experimental setup. The silicon surface barrier detector (SSB) and the large-area position-sensitive ionization chamber (LAPSIC) are used to detect the coincident fission fragments.

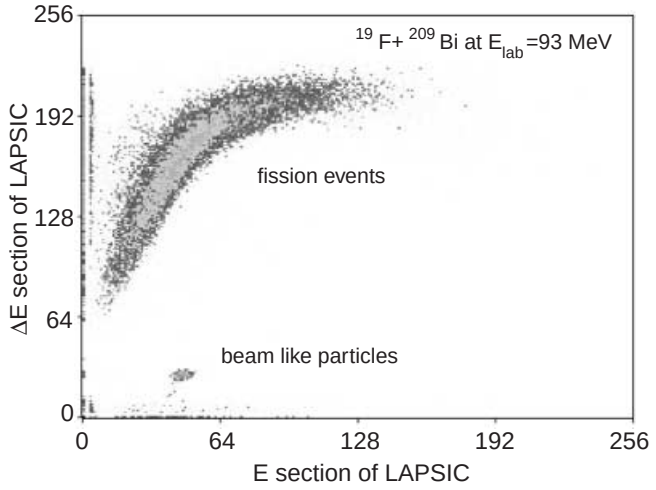

Fig. 2. 2D plot of the coincident fission events detected in the LAPSIC. The X and Y axes correspond to the pulse heights as observed in the E section and ΔE section of the LAPSIC, respectively for $^{19}\mathrm{F} + ^{209}\mathrm{Bi}$ at $E_{\mathrm{lab}} = 93$ MeV.

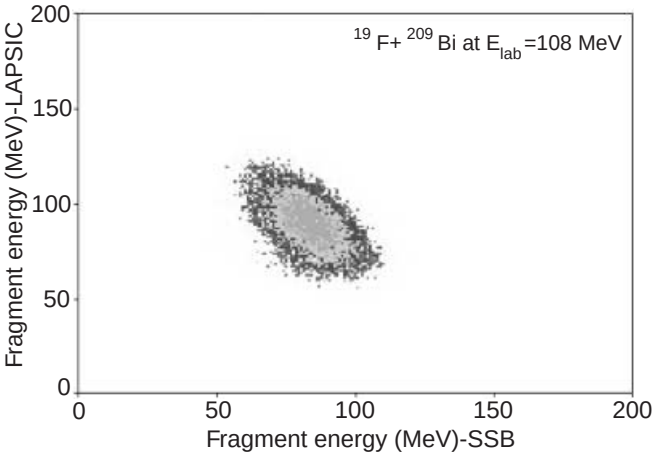

Fig. 3. 2D plot of the energy of the coincident fission fragments as observed in the two detectors. The X and Y axes correspond to the energy measured in SSB and LAPSIC, respectively for $^{19}\mathrm{F} + ^{209}\mathrm{Bi}$ at $E_{\mathrm{lab}} = 108$ MeV.

distributions of the fission fragments from the fission of secondary radioactive beams of the nuclei from ^{214}Rn to ^{234}U have been studied. The fission of these nuclei was caused by exciting the giant dipole resonance due to the electromagnetic interaction between the ion beam and the Pb target nuclei [11,12]. The experiments showed that, with increasing mass of the fissioning nucleus, a transition takes place from the predominantly symmetric to predominantly asymmetric fission in this region of nuclei at low excitation energies. Thus, the problem of mass, energy equilibration in heavy-ion–induced fission reactions is not yet fully understood.

In recent years, anomalous features have been reported in the fission fragment angular anisotropies at near barrier energies for many fissioning systems [4,13,14]. These have been interpreted to be due to occurrence of quasi-fission reactions when the projectile interacts with the tip of a deformed target nucleus leading to non-equilibration in the K distribution of the fissioning nucleus. There have been also some reports of anomalous behaviour of fragment angular distributions for certain target-projectile combinations even with nearly spherical target nuclei such as ^{209}Bi [15] and ^{208}Pb [16]. Recently, Samant *et al.* [17] observed fission fragment anisotropies in $^{19}\mathrm{F} + ^{209}\mathrm{Bi}$ system in agreement with the saddle point statistical model calculations over a range of bombarding energies, thereby concluding that the spherical target plus projectile system behave normal from near to above barrier energies. This observation is in contrast to the findings of Hinde *et al.* [18] where they measured fusion cross-sections for $^{19}\mathrm{F} + ^{208}\mathrm{Pb}$, which is also a spherical system, and have reported that statistical model calculations of the fission anisotropies were unable to reproduce the observed dependence on beam energy. In the presence of such conflicting results as regard to spherical targets and also because there have not been many studies on the mass, energy correlations of the fission fragments in these systems, we were motivated in the present work to measure the mass and total kinetic energy distributions of the fission fragments in $^{16}\mathrm{O},^{19}\mathrm{F} + ^{209}\mathrm{Bi}$ systems over a wide range of excitation energies ($E^* = 30$–50 MeV). Section 2 gives the details of the experimental setup and the data analysis procedure. Section 3 contains the results of the present work and sect. 4 discusses the random neck rupture model calculations with reference to the present results. The summary and conclusions are given in sect. 5.

2 Experimental setup and data analysis

The experiments were carried out at the 14MV BARC-TIFR Pelletron Accelerator Facility at Mumbai. Figure 1 shows the schematic diagram of the experimental setup. A

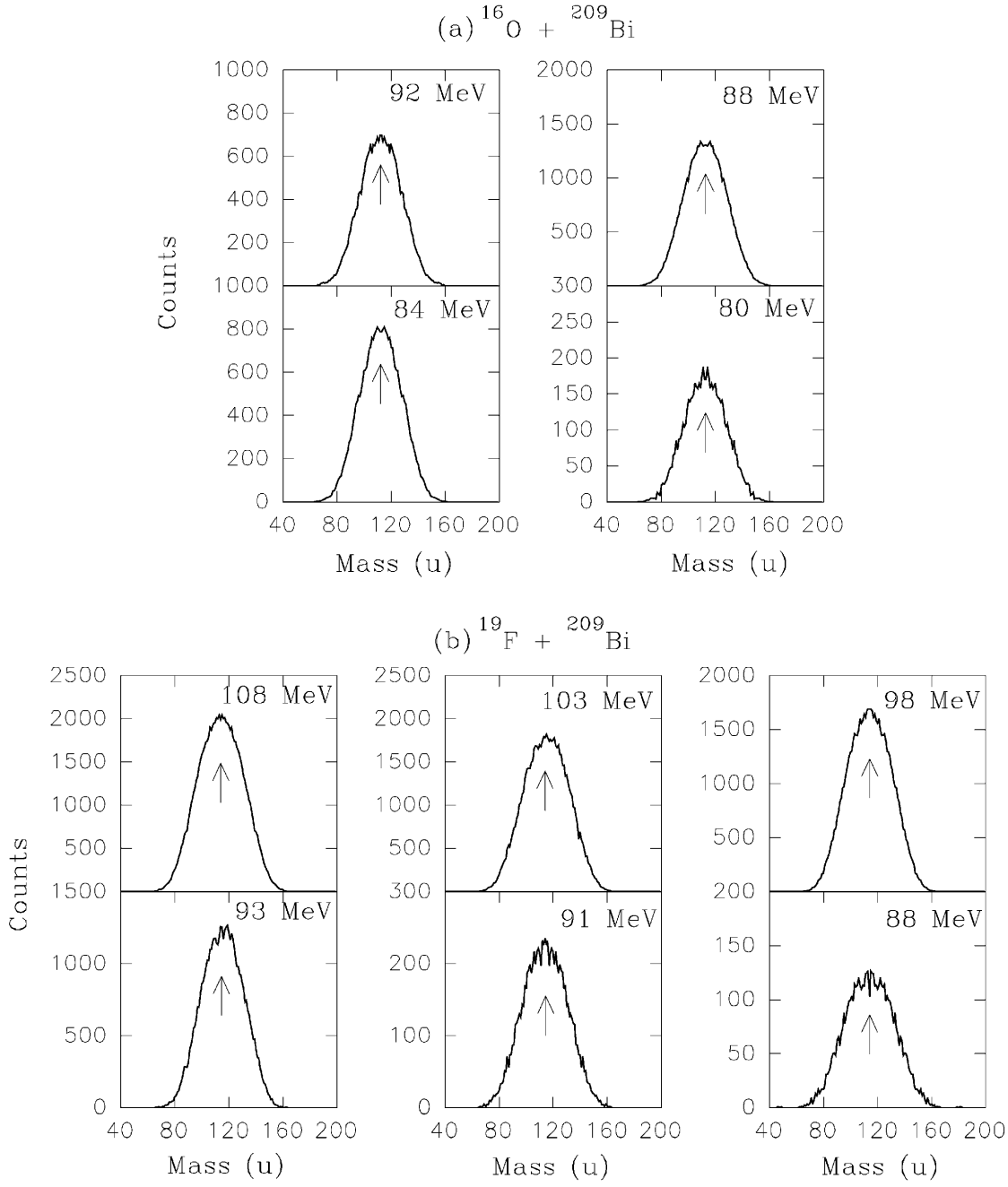

Fig. 4. Mass distributions for (a) $^{16}O + ^{209}Bi$ and (b) $^{19}F + ^{209}Bi$ systems for different projectile energies. The vertical arrows mark the position of $A_{CN}/2$ for the two systems.

self-supporting ^{209}Bi target (600 μg/cm^2) was bombarded with ^{16}O and ^{19}F beams with energies ranging from above barrier to below barrier energies. The fission fragments were detected using the combination of a 60 μm silicon surface barrier detector (SSB) and a large-area position-sensitive ionization chamber (LAPSIC), kept on either side of the beam to detect simultaneously the complementary fragments. The LAPSIC is a multi anode ionization chamber in which the first three sections were shorted to give partial energy loss (ΔE) of the fission fragments. The residual energy (E) of the fission fragments was measured in the last anode section. The working and performance characteristics of LAPSIC have been discussed elsewhere [19,20]. The SSB detector was kept at an angle of 70° with respect to the beam direction, whereas the ionization chamber was placed at a mean angle of 90° on the opposite side to cover the average folding angle of the complementary fragments expected for these reactions. The angular openings of the surface barrier detector and the ionization chamber in the reaction plane were ±3° and ±11°, respectively, so that the fission folding angle distributions for full momentum transfer for both the systems were

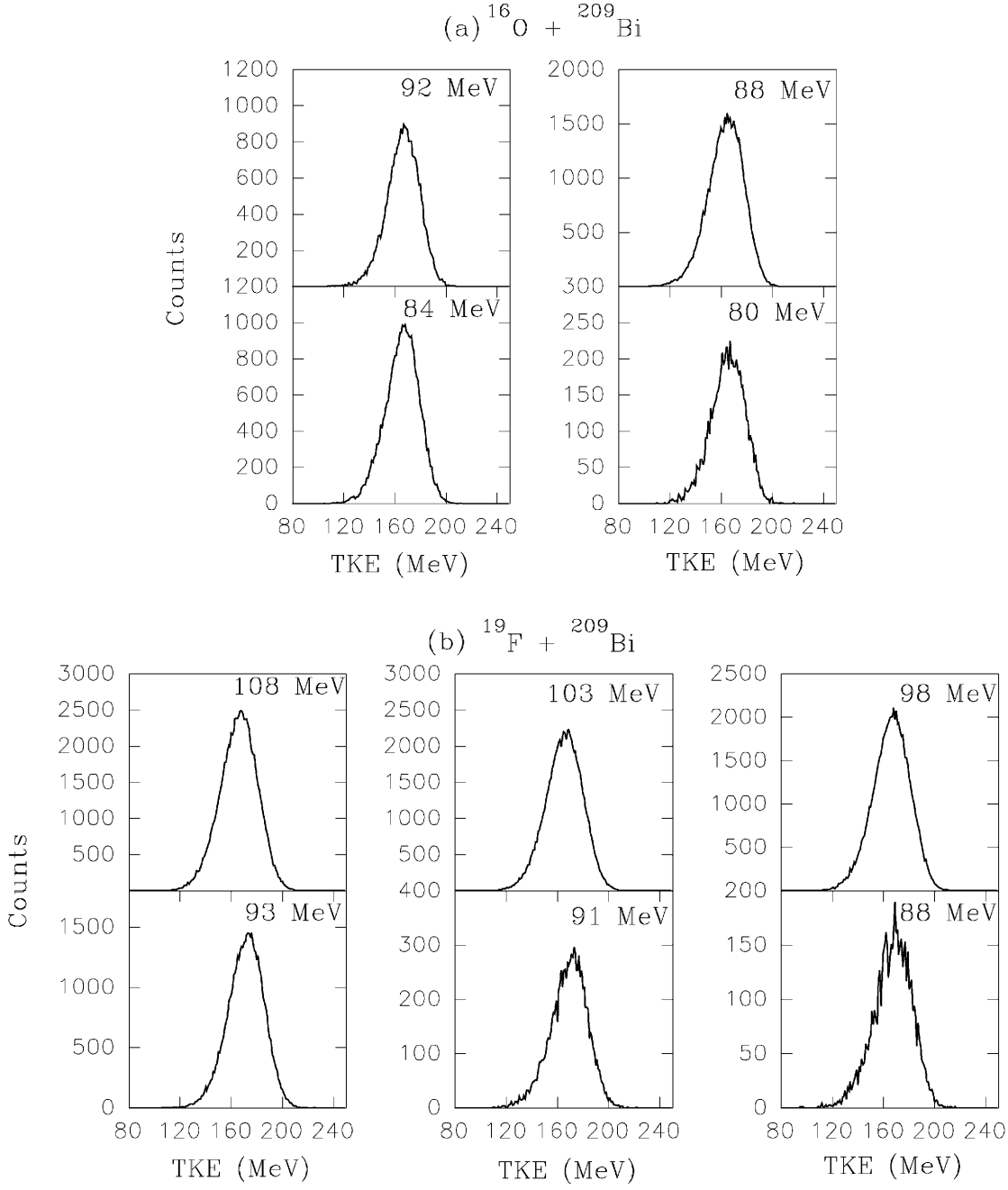

Fig. 5. Total kinetic energy distributions for (a) $^{16}O + ^{209}Bi$ and (b) $^{19}F + ^{209}Bi$ systems for different projectile energies.

reasonably well covered by the detectors at various bombarding energies. The component of transfer-induced fission is expected to be quite small due to large fission barrier heights ($\sim$ 10 to 12 MeV) of the target-like fissioning nuclei in this mass region. For the present detector geometry, we have simulated the folding angle distributions and the mass and total kinetic energy distributions at various bombarding energies for $^{16}O + ^{209}Bi$ and $^{19}F + ^{209}Bi$ reactions, in order to ensure that there is no biasing of the results due to the finite angular coverage of the detectors. It is shown that the angular coverage of the detectors in the present geometry is sufficient for a proper determination of the kinetic energy and mass distributions of the fission fragments for both the systems. The simulation results have been discussed in detail in Appendix 1. The ionization chamber was operated at a pressure of 21 mbar of P-10 gas in flow mode. The ΔE and E signals from the ionization chamber and the energy signals from the silicon surface barrier detector were recorded event by event for further off-line analysis. The fission fragments detected in LAPSIC appear as a well-separated band in the ΔE-E plot, as shown in fig. 2. To detect the coincident binary fragments a time correlation was established by taking the start signal from the SSB and stop signal from the

LAPSIC using a time to amplitude converter. The elastic scattering events are further eliminated by the application of a gate on time correlation signal on the 2D plot of the energy of the fragments as observed in the two detectors, as shown in fig. 3. The energy calibration of the detectors for fission fragments was done using a ^{252}Cf spontaneous-fission source. The pulse heights from the two detectors were converted into the post-scission kinetic energies of the two fragments by an event-by-event iterative analysis. A mass-dependent energy calibration procedure was used to correct for the pulse height defect in the surface barrier detector, using the parameters given by Wiessenberger *et al.* [21]. The corrections due to energy loss in the target foil, polypropylene window and the gas dead layer at the entrance of the ionization chamber were incorporated in the data analysis to determine the energies of the fission fragments. The total average energy loss for the most probable fragments in the ^{209}Bi target, the polypropylene window and the gas dead layer of the chamber was seen to be in the range of 15–20 MeV, which could be corrected in the present analysis. The center-of-mass energies of the fragments were derived after kinematic transformation assuming full momentum transfer to the compound nucleus. These energies were further corrected for neutron evaporation effects to obtain the preneutron emission masses by using the mass and momentum conservation relations. For neutron emission corrections, we have taken the available data on the systematics for post-scission neutron multiplicities as a function of the fissility [22,23] and assuming the neutron emission to be proportional to the fragment masses. The corrections due to neutron emission were found to be of the order of 1.5 to 2.0 MeV. After applying all the corrections discussed above, the kinetic energy and mass distributions of the fission fragments, measured by the two detectors, were found to agree well with each other, implying that the correction factors in both the detectors have been taken into account in a consistent manner.

3 Results and discussion

Figure 4 shows the measured fragment mass distributions for the $^{16}\mathrm{O} + ^{209}\mathrm{Bi}$ and $^{19}\mathrm{F} + ^{209}\mathrm{Bi}$ reactions for different bombarding energies of the projectile. These distributions correspond to the average of the distributions measured in the two detectors. The vertical arrows in the figure mark the position of symmetric fission at $A_{CN}/2$ for the two systems. It is observed that the mass distributions are, in general symmetric in shape peaking around $A_{CN}/2$. The mass distribution widths are observed to be generally higher for the $^{19}\mathrm{F} + ^{209}\mathrm{Bi}$ system as compared to the $^{16}\mathrm{O} + ^{209}\mathrm{Bi}$ system as would be expected due to difference in the fissility of the two systems. The width of the mass distributions were determined by fitting the spectra with Gaussian distributions, and are discussed below. Figure 5 shows the total fragment kinetic energy distributions for both $^{16}\mathrm{O} + ^{209}\mathrm{Bi}$ and $^{19}\mathrm{F} + ^{209}\mathrm{Bi}$ reactions at various bombarding energies. These distributions are also seen to be nearly symmetric in shape. The average and

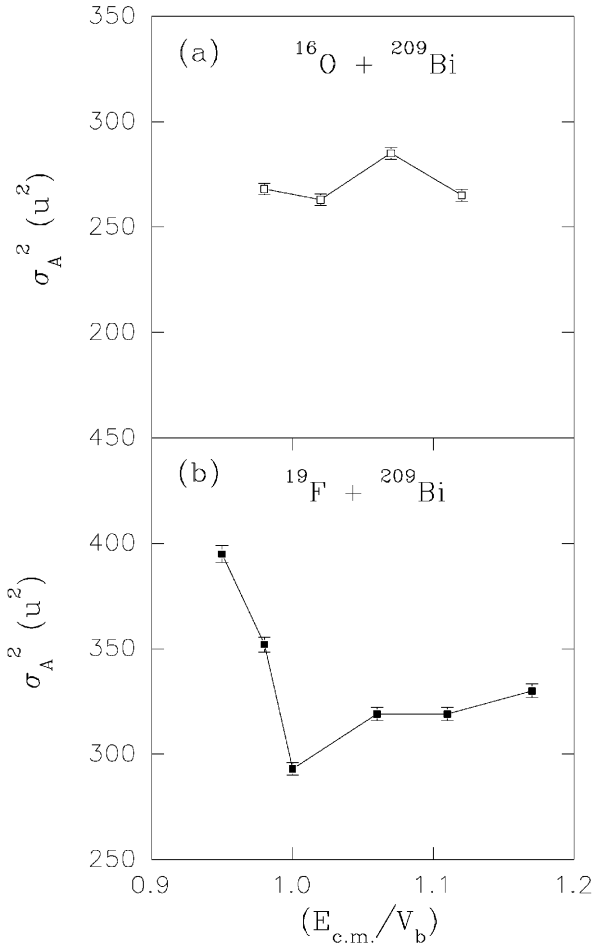

Fig. 6. Mass variance σ_A^2 as a function of $(E_{\mathrm{c.m.}}/V_{\mathrm{b}})$ for (a) $^{16}\mathrm{O} + ^{209}\mathrm{Bi}$ and (b) $^{19}\mathrm{F} + ^{209}\mathrm{Bi}$ systems.

width of these distributions were also obtained by fitting the data with Gaussian distributions. It was verified that the values obtained by the fitting procedure are very close to those derived by taking the first and second moments of the distributions.

Figure 6 shows the variance, σ_A^2 of the fragment mass distributions as a function of the bombarding energy. The data have been plotted for both the systems as a function of $E_{\mathrm{c.m.}}/V_{\mathrm{b}}$, where V_{b} is the fusion barrier as determined by coupled-channel calculations. It is seen that in case of the $^{16}\mathrm{O} + ^{209}\mathrm{Bi}$ system, the variance of the mass distribution, σ_A^2 remains nearly flat with variation in $E_{\mathrm{c.m.}}/V_{\mathrm{b}}$, whereas for the $^{19}\mathrm{F} + ^{209}\mathrm{Bi}$ system, σ_A^2 initially has a slow decrease with decrease in the bombarding energy up to the barrier energy, and then rises sharply at below barrier energies. The experimentally observed values for σ_A^2 at above barrier energies match well with the available systematics for the compound nuclei populated close to the present systems. Hinde *et al.* [24] observed $\sigma_A^2 = 304$ u^2 for $^{20}\mathrm{Ne} + ^{209}\mathrm{Bi}$ at $E_{\mathrm{lab}} = 149$ MeV. Similarly, Itkis *et al.* [25] observed $\sigma_A^2 = 224$ u^2 for $^{16}\mathrm{O} + ^{208}\mathrm{Pb}$ at $E_{\mathrm{lab}} = 108$ MeV. The present results for σ_A^2 are, however, somewhat higher than that reported by Choudhury

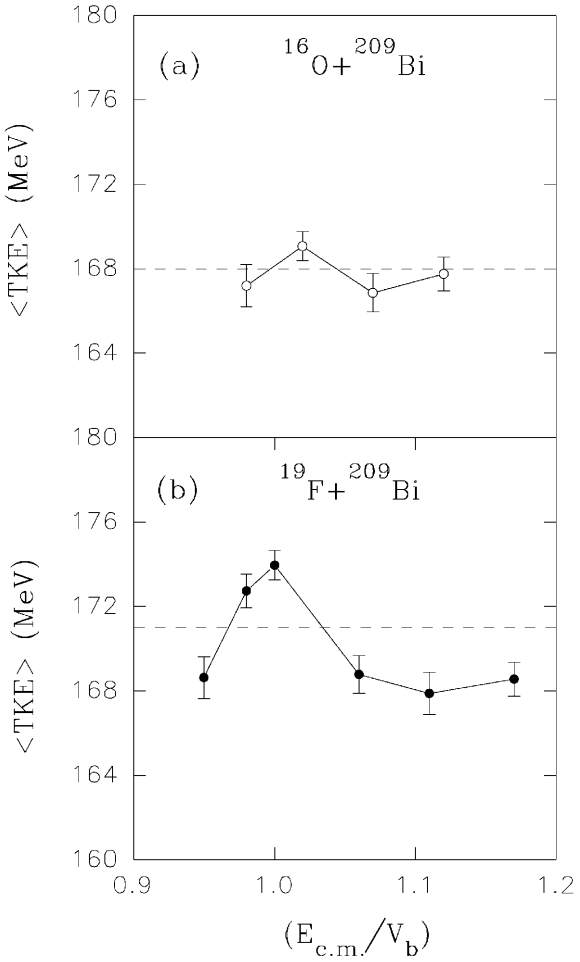

Fig. 7. Average total kinetic energy $\langle TKE \rangle$ as a function of $(E_{\mathrm{c.m.}}/V_{\mathrm{b}})$ for (a) $^{16}\mathrm{O} + ^{209}\mathrm{Bi}$ and (b) $^{19}\mathrm{F} + ^{209}\mathrm{Bi}$ systems. Dashed lines show the $\langle TKE \rangle$ values expected from Viola's systematics for the two systems.

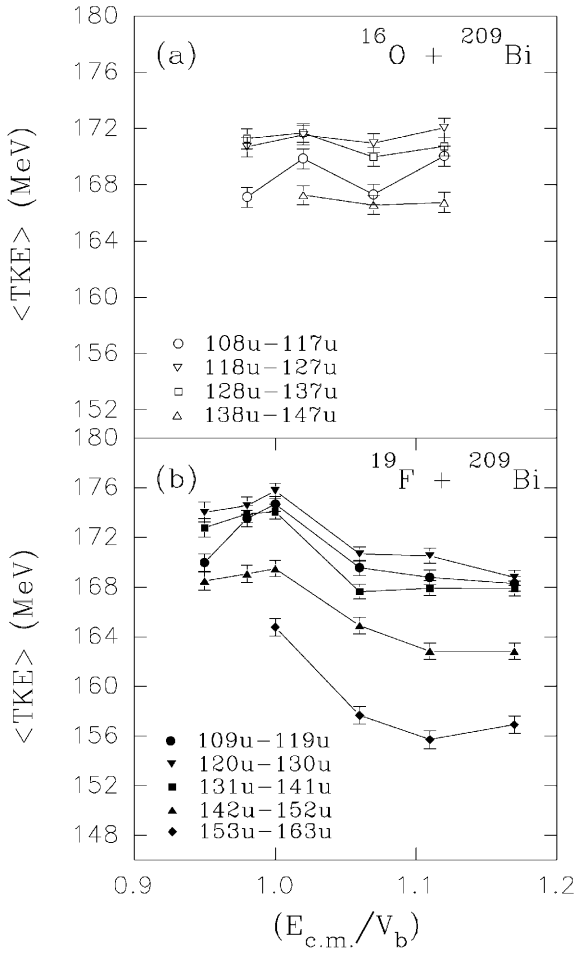

Fig. 8. Average total kinetic energy $\langle TKE \rangle$ as a function of $(E_{\mathrm{c.m.}}/V_{\mathrm{b}})$ for (a) $^{16}\mathrm{O} + ^{209}\mathrm{Bi}$ and (b) $^{19}\mathrm{F} + ^{209}\mathrm{Bi}$ systems for different mass bins. Each mass bin for $^{16}\mathrm{O} + ^{209}\mathrm{Bi}$ is shown with an open symbol and for $^{19}\mathrm{F} + ^{209}\mathrm{Bi}$ with a closed symbol.

et al. [26] for the $^{16}\mathrm{O}+^{209}\mathrm{Bi}$ system, where σ_A^2 values were measured to be in the range of 125 to 150 u^2, using velocity measurements. The corrections applied in double-energy measurements are generally larger than that applied for double-velocity measurements [27] and this may be the cause for higher mass variances seen in the present work, as compared to that reported by Choudhury *et al.* The present observation of a sharp rise in the width of the mass distribution for the $^{19}\mathrm{F} + ^{209}\mathrm{Bi}$ system at the sub-barrier energies is quite interesting, and as will be shown below, this result correlates with the variation of the fragment kinetic energy with the bombarding energy at near barrier energy for this system.

Figure 7 shows the variation of the average total kinetic energy $\langle TKE \rangle$, with $(E_{\mathrm{c.m.}}/V_{\mathrm{b}})$ for the two systems. The error bars shown include the statistical errors along with the errors from the uncertainties in estimating the energy loss in the target, polypropylene window and the kinematic corrections. The dashed lines in the figure correspond to the average TKE expected on the basis of Viola's systematics. It is seen that for $^{16}\mathrm{O} + ^{209}\mathrm{Bi}$ (fig. 7a), the variation in $\langle TKE \rangle$ with $(E_{\mathrm{c.m.}}/V_{\mathrm{b}})$ is almost flat within the experimental uncertainties and follows Viola's systematics. For the $^{19}\mathrm{F} + ^{209}\mathrm{Bi}$ system (fig. 7b), a peaking behaviour is seen in the total fragment kinetic energy near the barrier. At above barrier energies the average kinetic energy of the fragments are 2–3 MeV lower than Viola's systematics for this system. As has been already pointed out earlier, the energy measurements have been done in an absolute manner using the ^{252}Cf data, adopting the same procedure for both $^{16}\mathrm{O} + ^{209}\mathrm{Bi}$ and $^{19}\mathrm{F} + ^{209}\mathrm{Bi}$ systems. The relatively strong variation of $\langle TKE \rangle$ with bombarding energy in the near barrier region for the $^{19}\mathrm{F} + ^{209}\mathrm{Bi}$ system is quite intriguing, but seems to be real.

Such a behaviour is also seen to be present in varying degrees for different mass splits as is evident from fig. 8, where the $\langle TKE \rangle$ is plotted as a function of the bombarding energy for different mass bins for both $^{16}\mathrm{O} + ^{209}\mathrm{Bi}$ and $^{19}\mathrm{F} + ^{209}\mathrm{Bi}$ systems. The size of the mass bin is 10 mass units and each mass bin is represented with a different symbol for the two systems. It is observed that for the $^{19}\mathrm{F} + ^{209}\mathrm{Bi}$ system (fig. 8(b)), the peak-like structure in $\langle TKE \rangle$ is present for all the mass bins at near barrier

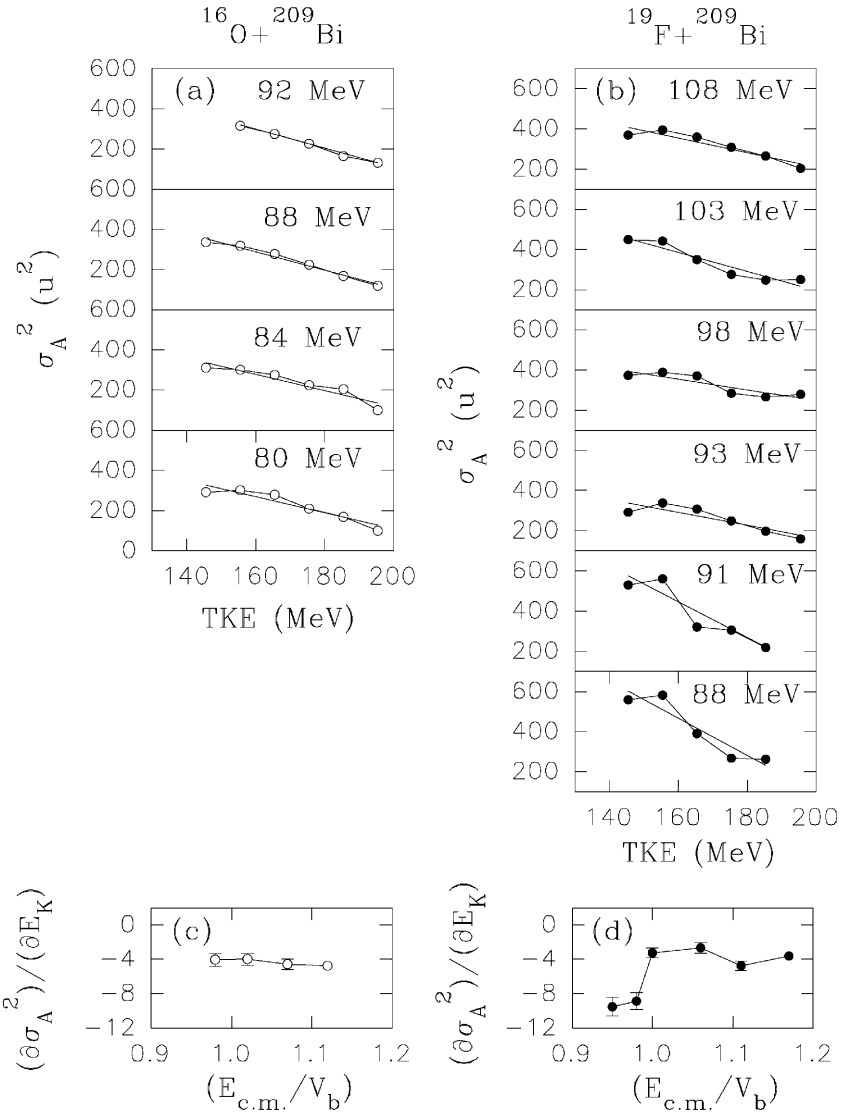

Fig. 9. Variation of mass variance σ_A^2 with total kinetic energy for various beam energies for (a) ^{16}O+^{209}Bi and (b)^{19}F+^{209}Bi systems. The linear fits to the data points are shown as straight continuous lines. (c) and (d) show the slope parameter, $\partial\sigma_A^2/\partial E_K$ as a function of $(E_{\rm c.m.}/V_{\rm b})$ for ^{16}O + ^{209}Bi and ^{19}F + ^{209}Bi systems, respectively. The line joining the points is just an eye guide.

energy. For the ^{16}O+^{209}Bi system, the variation in $\langle TKE\rangle$ remains nearly flat with the bombarding energy for every mass bin. It is also observed that for a given bombarding energy, the value of $\langle TKE\rangle$ generally decreases with increasing mass asymmetry, as is expected from the Coulomb energy and Q-value considerations. It is also seen that at any given bombarding energy, the $\langle TKE\rangle$ values are somewhat lower for symmetric mass divisions as compared to moderate mass asymmetric splits corresponding to the heavy fragments in the doubly closed shell region of $Z = 50$ and $N = 82$. The influence of this shell is known to be quite dominant in low-energy fission, and its effect is still seen in the excitation energy range of 30–50 MeV, studied in the present work.

Figures 9(a) and 9(b) show the variation of σ_A^2 with TKE for^{16}O+^{209}Bi and ^{19}F+^{209}Bi systems, respectively, for various beam energies. A TKE bin size of 10 MeV was selected for this analysis. It is seen that in general, for both the systems, σ_A^2 decreases with increasing TKE. The decrease in σ_A^2 with TKE is consistent with the temperature dependence expected of σ_A^2 [28], as higher TKE values would correspond to lower excitation energy or temperature in the fissioning system at the scission point. The linear fits to the data points are shown as straight lines. It is also noticed that the slope $\partial\sigma_A^2/\partial E_K$ has a nearly constant value of about $(\partial\sigma_A^2/\partial E_K) \sim -4$ amu^2/MeV for the ^{16}O + ^{209}Bi system over the full bombarding energy range (fig. 9(c)). In marked contrast, the behaviour of the slope parameter for ^{19}F + ^{209}Bi system is quite different. For the ^{19}F + ^{209}Bi system, $\partial\sigma_A^2/\partial E_K$ remains nearly constant [$(\partial\sigma_A^2/\partial E_K) \sim -4$ amu^2/MeV] at above barrier energies and suddenly shows a dip to a value of

$[(\partial\sigma_A^2/\partial E_K) \sim -8$ amu^2/MeV] as the bombarding energy is reduced below the barrier (fig. 9(d)). This result seems quite interesting, which may also signal to a change in the fission mechanism in the ^{19}F + ^{209}Bi system at sub-barrier energies. From the above discussions, it is evident that the fragment mass-energy distributions and their correlations in the ^{19}F + ^{209}Bi reaction exhibit quite unexpected features at sub-barrier energies as compared to the ^{16}O + ^{209}Bi reaction. These results can serve as important inputs for providing a full dynamical description of the fusion-fission reaction process in these systems. In the following, however, we apply one of the existing scission point models for a qualitative understanding of certain features of mass-energy correlations in a limited way.

4 Calculations for the average and variance of the TKE distribution: Brosa's Random Neck Rupture Model

We have applied Brosa's formalism [29] of random neck rupture to correlate some of the present experimental findings. The most important feature of the random neck rupture model is the prescission shape of the nucleus characterized by its semilength l. The model can be used to calculate quantities such as mass yield $Y(A)$, the neutron multiplicity $\overline{\nu}(A)$ and the total kinetic energy $TKE(A)$, if one knows the elongation of the nucleus ($2l$) prior to scission. $\langle TKE\rangle$ can be used as an inverse measure of the length of the prescission shape. High TKE indicates a short prescission shape and low TKE corresponds to a longer prescission shape. We give below a brief discussion of Brosa's model without going into the full explanations of the various equations used in the calculations which can be found in ref. [29]. When the nucleus splits into two fragments, the potential energy consists of a Coulomb and a nuclear part. The $\langle TKE\rangle$ is obtained as

$$\langle TKE\rangle = V_{\rm Cou} + V_{\rm nuc} + K_{\rm s}\,, \tag{1}$$

where $K_{\rm s}$ is the prescission kinetic energy term and is taken to be of the order of 10 MeV [29]. The Coulomb part is given as

$$V_{\rm Cou} = \frac{e_0^2 Z(Z_{CN}-Z)}{l} S(x_1,x_2)\,, \tag{2}$$

where $e_0^2 \sim 1.44$ MeV fm. The factor $S(x_1,x_2)$ contains the corrections due to spheroidal deformations. The quantities x_i are related to the eccentricities ε_i by

$$x_i = \frac{a_i\varepsilon_i}{l}, \qquad \varepsilon_i = \left[1-\left(\frac{b_i}{a_i}\right)^2\right]^{1/2}, \tag{3}$$

where a_i and b_i are the semiaxes of the two touching embedded spheroids which represent the newly born fragments. The nuclear interaction energy $V_{\rm nuc}$ between the nascent fragments is evaluated using the proximity formula [30] and is given by

$$V_{\rm nuc} = 4\pi\gamma_0\phi(0)\frac{b_1^2 b_2^2}{a_1 b_2^2 + a_2 b_1^2}\,, \tag{4}$$

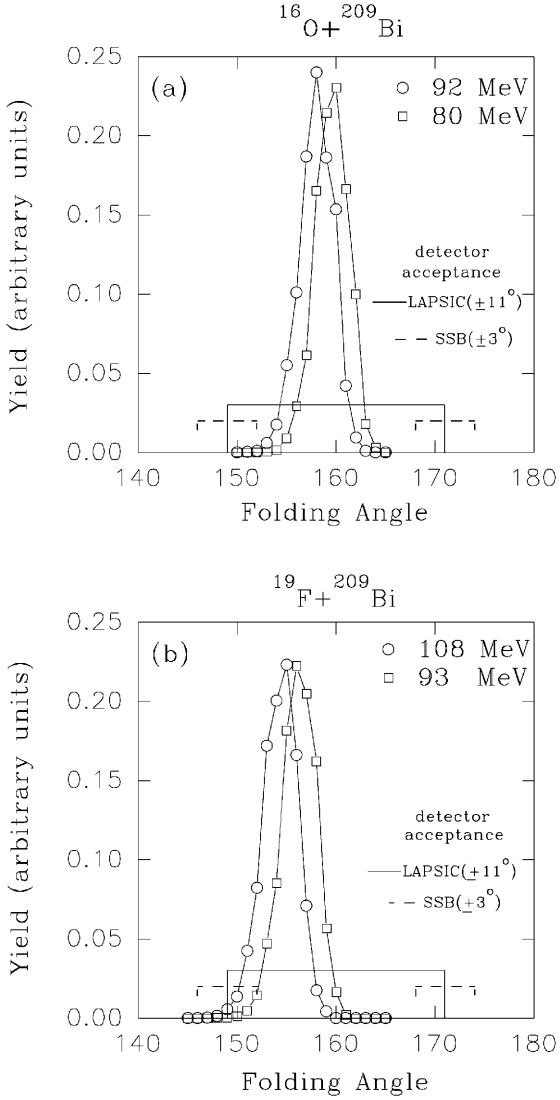

Fig. 10. Folding angle distributions for (a) ^{16}O+^{209}Bi system at $E_{\rm lab} = 80$, 92 MeV and (b)^{19}F + ^{209}Bi system at $E_{\rm lab} = 93$, 108 MeV alongwith the detector acceptance. The acceptance for LAPSIC is shown by straight continuous lines alongwith the angular spread of the SSB detector.

where a_1,a_2 and b_1,b_2 are the semiaxis of the nascent fragments. γ_0 is the surface tension coefficient and $\phi(0) = -1.7817$ fm is the value of the proximity potential function [30] for zero distance between the surfaces. Thus, knowing the experimental $\langle TKE\rangle$, one can calculate the semilength at the scission point. Table 1 summarises the relevant parameters of the calculation along with the results obtained for the ^{16}O + ^{209}Bi and ^{19}F + ^{209}Bi systems at various bombarding energies.

For calculating the variances in TKE, we have used the standard Langevin equation, keeping the semilength l as an essential degree of freedom, as per the prescription given by Brosa *et al.* [29]. It is given by the relation

$$\sigma_{E_K}^2 = \sigma_{E_{K,c}}^2 + \sigma_{E_{K,v}}^2 - 2\sigma_{E_{K,m}}^2\,, \tag{5}$$

Table 1. Relevant parameters for the systems studied: $E_{\rm lab}$: projectile energy in laboratory; $E^*_{\rm sad}$: excitation energy of the compound nucleus at the saddle point; T: nuclear temperature at the saddle point using a level density parameter $a = A_{CN}/10$ MeV^{-1}; $\langle TKE\rangle$: experimentally measured total kinetic energy; l: semilength at scission; $\sigma^{\rm exp}_{E_K}$: experimentally measured variance in $\langle TKE\rangle$; $\sigma^{\rm th}_{E_K}$: theoretical values for variance in $\langle TKE\rangle$ as per Brosa's prescription.

System	$E_{\rm lab}$ (MeV)	$E^*_{\rm sad}$ (MeV)	T (MeV)	$\langle TKE\rangle$ (MeV)	l (fm)	$\sigma^{\rm exp}_{E_K}$ (MeV)	$\sigma^{\rm th}_{E_K}$ (MeV)
1	2	3	4	5	6	7	8
^{16}O + ^{209}Bi	80	22	0.99	167 ± 1.0	17.8	14.0 ± 0.8	14.4
	84	26	1.07	169 ± 0.7	17.6	13.4 ± 0.3	15.2
	88	29	1.14	167 ± 0.9	17.8	14.1 ± 0.3	15.4
	92	33	1.21	168 ± 0.8	17.7	12.4 ± 0.3	16.0
^{19}F + ^{209}Bi	88	27	1.09	169 ± 1.0	17.9	14.9 ± 0.6	13.4
	91	30	1.15	173 ± 0.8	17.6	13.9 ± 0.4	14.1
	93	32	1.18	174 ± 0.7	17.5	14.1 ± 0.2	14.3
	98	36	1.26	169 ± 0.9	17.9	14.9 ± 0.2	14.4
	103	41	1.34	168 ± 1.0	18.0	14.7 ± 0.2	14.8
	108	46	1.42	169 ± 0.8	17.9	14.8 ± 0.2	15.3

$\sigma^2_{E_{K,c}}$ and $\sigma^2_{E_{K,v}}$ are the standard deviations of TKE due to fluctuations of length and velocity (defined as $\partial l/\partial t$). The mixed term $\sigma^2_{E_{K,m}}$ embodies correlation between length and velocity fluctuations. This correlation diminishes the variance thereby decreasing the Coulomb repulsion for increasing scission length. The mathematical formulations for $\sigma^2_{E_{K,c}}$, $\sigma^2_{E_{K,v}}$ and $\sigma^2_{E_{K,m}}$ are given as

$$\sigma^2_{E_{K,c}} = V_{\rm Cou}\frac{\Delta l}{l}\left(\frac{2T}{\Delta U}\right)^{1/2}\psi_l(x)\,, \tag{6}$$

$$\sigma^2_{E_{K,v}} = (T\Delta U)^{1/2}\psi_v(x)\,, \tag{7}$$

$$\sigma^2_{E_{K,m}} = \left(V_{\rm Cou}\frac{\Delta l}{l}T\right)^{1/2}\psi_m(x)\,, \tag{8}$$

where $\psi_l(x)$, $\psi_v(x)$ and $\psi_m(x)$ are the dimensionless functions depending on the friction parameter x. T is the temperature of the nucleus at the saddle point, ΔU is the drop in potential energy and Δl is the change in the semilength from saddle to scission. For the present systems, the friction parameter x was taken to be 1.7. The value of the friction parameter and the dimensionless functions have been taken as per Brosa's formalism [29]. The fraction $K_S/\Delta U$ ($\sim \Phi(x)$) of the potential energy that turns into kinetic energy fixes the friction parameter x. The excitations caused by the friction on the way from barrier to scission is defined by $\Phi(x)$ and for our systems corresponding to $A_{CN} < 250$, $\Phi(x) = 0.375$ which gives $x = 1.7$. The values of the dimensionless functions are obtained as: $\psi_l(x) = 0.788$, $\psi_v(x) = 0.855$ and $\psi_m(x) = 0.786$. The semilength of the stretched complex at the saddle has been calculated as per the formalism of Hasse and Myers [31] and the effective moment of inertia at the saddle point, $J_{\rm eff}$ thus derived is in very close agreement with the prescription given by Sierk [32]. The calculated values of the semilength, l are given in column 6 of table 1. Column 8 gives the values for $\sigma^{\rm th}_{E_K}$ (calculated), using the above prescription, which matches closely with the experimental values $\sigma^{\rm exp}_{E_K}$ (column 7, table 1) indicating that the semilength values derived from experimental $\langle TKE\rangle$ are consistent with another independent experimental observation, *i.e.* $\sigma^{\rm exp}_{E_K}$. Brosa's formalism proposes that several prescission shapes can be formed. At least three prescission shapes are prescribed: standard, superlong and supershort. Standard shape is slightly asymmetric and of normal length while superlong and supershort shapes are both almost symmetrical and appreciably longer or shorter than the standard one. The difference between the shapes lies in their mean length. An admixture of such shapes in the exit channel can influence the $\langle TKE\rangle$ released in fission. Although the above model provides a framework for explaining the average and width of the TKE distributions in a consistent way, the exact mechanism of the fission process, giving rise to different scission shapes, requires full dynamical calculations of the fusion-fission path in heavy-ion collisions. We have only given a schematic discussion of the theoretical-model calculations based on the random neck rupture model, and do not attempt here to explain all the observed features in the mass and energy distributions of the fission fragments in the two reactions. The present experimental results on the mass, energy correlations of fission fragments in the different fissioning systems should prove to be important from the point of testing the full dynamical calculations of the fusion-fission process in heavy-ion–induced reactions. Also it would be of interest to experimentally measure the mass-energy correlations for other systems at near and sub-barrier energies using different target-projectile combinations for a systematic understanding of the fusion-fission mechanism in heavy-ion reactions.

5 Summary and conclusion

The fragment mass and kinetic energy distributions and the correlations between them have been studied in ^{16}O + ^{209}Bi and ^{19}F + ^{209}Bi reactions. It is observed that in

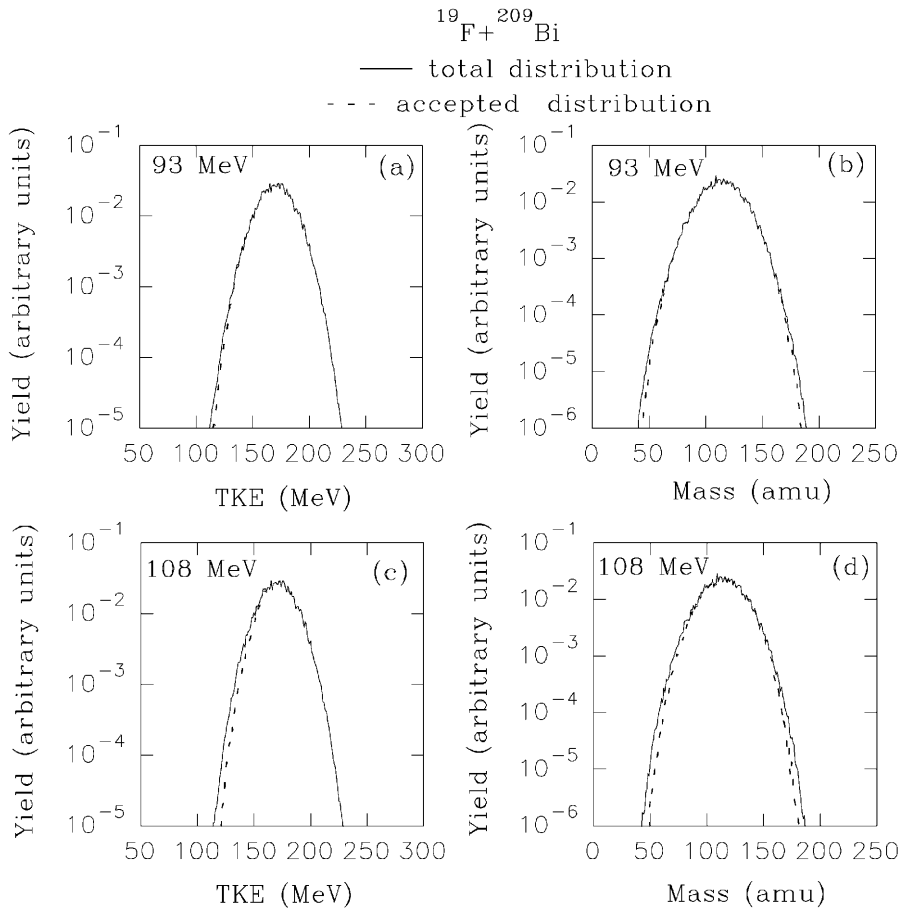

Fig. 11. Simulated calculations for TKE and mass distribution for $^{19}\mathrm{F}+^{209}\mathrm{Bi}$ reaction showing the overlap of the total events (continuous lines) and the accepted events (dashed lines). The yields in arbitrary units are shown in lograthmic scale. (a) TKE distributions and (b) mass distributions corresponding to 93 MeV of bombarding energy. (c) and (d) correspond to the results for 108 MeV bombarding energy.

the $^{19}\mathrm{F}+^{209}\mathrm{Bi}$ reaction there is an enhancement in the $\langle TKE\rangle$ of the fission fragments at near barrier bombarding energies, in contrast to the case of $^{16}\mathrm{O}+^{209}\mathrm{Bi}$, where the $\langle TKE\rangle$ is seen to be independent of the bombarding energy. The enhancement in $\langle TKE\rangle$ is correlated with a reduced mass width at the barrier for the $^{19}\mathrm{F}+^{209}\mathrm{Bi}$ reaction. In the sub-barrier region σ_A^2 shows a sharp rise in the case of $^{19}\mathrm{F}+^{209}\mathrm{Bi}$ reaction. Another interesting experimental observation is the bombarding energy dependence of the slope of the variation of the mass width with TKE. In case of the $^{16}\mathrm{O}+^{209}\mathrm{Bi}$ reaction, this slope is nearly constant over the bombarding energy range studied in the present work. However, for the $^{19}\mathrm{F}+^{209}\mathrm{Bi}$ reaction, this slope shows an abrupt drop at the sub-barrier energies. It has also been observed in recent experiments [10–12], that there is a clear evidence for a transition from double humped to single humped mass distributions in low-energy fission around $A_{CN}=226$. Systems with $A_{CN}<226$ end up in predominantly single humped distributions, whereas systems with $A_{CN}>226$ predominantly show double humped distributions when fissioning with low excitation energies. The two systems,$^{16}\mathrm{O}+^{209}\mathrm{Bi}$ and $^{19}\mathrm{F}+^{209}\mathrm{Bi}$ investigated in the present work are just below and above this limit, respectively. A contribution of asymmetric fission in the heavier system could lead to the increased width of the mass distributions in the low-energy region. The varying influence of spherical ($N=82$, $Z=50$) and deformed ($N=88$, $Z=60$) shells in these mass regions could also give rise to differences in the mass-energy correlations observed in these two systems.

We have applied Brosa's model of random neck rupture to explain the $\langle TKE\rangle$ and the width of the TKE distribution. According to this model, several prescission shapes can be populated and TKE fluctuations can be caused by varying the semilength l of the prescission shape. Superposition of various contributions gives the $\langle TKE\rangle$ value which could be compared with the experiments. The enhanced anticorrelation in $\langle TKE\rangle$ *versus* σ_A^2 could be a manifestation of preponderence of supershort states [29] having reduced prescission lengths compared to the standard shapes, at near barrier energies for the $^{19}\mathrm{F}+^{209}\mathrm{Bi}$ system. Although this model has been applied to provide a general framework for calculating the kinetic energy and mass distributions, a detailed explanation of the present results would require full dynamical calculations of the fusion-fission process in various target-projectile systems.

The present results would prove to be important from the point of testing various dynamical models of the fusion-fission process. It is also necessary to investigate the mass-energy correlations for other target-projectile systems to obtain a systematic understanding of the reaction mechanisms involved in the heavy-ion fusion-fission process.

The authors are thankful to Dr. S.S. Kapoor for many helpful discussions on this work. They also acknowledge the help of B.V. Dinesh, R.G. Thomas, B.K. Nayak, V.P. Singh and A.L. Inkar during the course of the experiment. The help from the Pelletron accelerator staff for smooth running of the accelerator and providing necessary beams is gratefully acknowledged.

Appendix A. Simulations of the acceptance of LAPSIC detector for the correlated binary events

For the detector geometry employed in the present measurements, we have carried out detailed Monte Carlo simulations for the mass and total kinetic energy distributions at various bombarding energies for $^{16}O + ^{209}Bi$ and$^{19}F + ^{209}Bi$ reactions for calculating the acceptance of LAPSIC detector for the full folding angle distributions of the binary fission events. The simulations also include angular smearing effects for small-angle scattering in the target, neutron evaporation from the fragments and finite ($\pm 3^{\circ}$) angular coverage of the SSB detector. The simulation results show that the detector acceptance for the folding angle coverage is quite good for both the reactions.

The typical folding angle distributions are plotted in fig. 10(a) and 10(b) for certain typical bombarding energies for both the systems. Figure 10(a) shows the folding angle distributions for $^{16}O + ^{209}Bi$ system at 80 MeV and 92 MeV of bombarding energy. Figure 10(b) shows the folding angle distributions for $^{19}F + ^{209}Bi$ system at 93 MeV and 108 MeV of bombarding energy. The acceptance of LAPSIC and SSB are shown, respectively, as straight continuous and dashed lines. It is seen that the detectors are quite optimally placed for the $^{16}O + ^{209}Bi$ system. For the$^{19}F + ^{209}Bi$ system, a slight restriction for acceptance of asymmetric mass divisions may be present for the highest bombarding energies. This is further illustrated by the following graphs on the mass and TKE distributions obtained from the simulation calculations. Figure 11(a) to 11(d) show the mass and TKE distributions for the $^{19}F + ^{209}Bi$ reaction for the total and accepted events at the bombarding energies of 93 MeV and 108 MeV. The continuous lines correspond to the total simulated events and the dashed lines correspond to the actually accepted events in the detectors. The yield distributions have been plotted in logarithmic scale. It is seen that the percentage of events missing the detector coverage is 0.5 percent at 93 MeV of bombarding energy and 5.9 percent at 108 MeV of bombarding energy. As seen from figs. 11(a) to 11(d), this does not introduce any bias in the determination of the average and width of the mass and TKE distributions measured by the present experiment. From these figures it is clear that in the energy region where we are reporting the anomalous variation in $\langle TKE \rangle$ for $^{19}F + ^{209}Bi$ system, there is no biasing by the detector acceptance due to the fixed geometry configuration.

References

1. J.V. Kratz, J.O. Liljenzin, A.E. Norris, G.T. Seaborg, Phys. Rev. C **13**, 2347 (1976).
2. R.K. Choudhury, A. Saxena, V.S. Ramamurthy, D.M. Nadkarni, S.S. Kapoor, Nucl. Phys. A **463**, 597 (1987).
3. C. Gregoire, R. Lucas, C. Ngo, B. Schurmann, H. Ngo, Nucl. Phys. A **361**, 443 (1981).
4. N. Majumdar, P. Bhattacharya, D.C. Biswas, R.K. Choudhury, D.M. Nadkarni, A. Saxena, Phys. Rev. Lett. **77**, 5027 (1996).
5. Y. El. Masri, F. Hanappe, J.C. Steckmeyer, V. Martin, G. Bizard, B. Borderie, R. Brou, J.F. Broundet, P. Duhamel, H. Fuchs, J.L. Laville, J. Peter, R. Regimbart, M. Rivet, B. Tamain, Tsan Ng Chan, Nucl. Phys. A **517**, 340 (1990).
6. L.M. Pant, A. Saxena, R.K. Choudhury, D.M. Nadkarni, Phys. Rev. C**54**, 2037 (1996).
7. I.V. Pokrovsky, L. Calabretta, M.G. Itkis, N.A. Kondratiev, E.M. Kozulin, C. Maiolino, E.V. Prokhorova, A. Ya. Rusanov, S.P. Tretyakova, Phys. Rev. C **60**, 041304 (1999).
8. M.G. Itkis, V.N. Okolovich, A. Ya. Rusanov, G.N. Smirenkin, Z. Phys. A **320**, 433 (1985).
9. M.G. Itkis, V.N. Okolovich, A. Ya. Rusanov, G.N. Smirenkin, Sov. J. Nucl. Phys. **41**, 544 (1985).
10. I.V. Pokrovsky, M.G. Itkis, J.M. Itkis, N.A. Kondratiev, E.M. Kozulin, E.V. Prokhorova, V.S. Salamatin, V.V. Pashkevich, S.I. Mulgin, A. Ya. Rusanov, S.V. Zhdanov, G.G. Chubarian, B.J. Hurst, R.P. Schmitt, C. Agodi, G. Bellia, L. Calabretta, K. Lukashin, C. Maiolino, A. Kelic, G. Rudolf, L. Stuttge, F. Hanappe, Phys. Rev. C **62**, 014615 (2000).
11. K.-H. Schmidt, A.R. Junghans, J. Benlliure, C. Böckstiegel, H.-G. Clerc, A. Grewe, A. Heinz, A.V. Ignatyuk, M. de Jong, G.A. Kudyaev, J. Müller, M. Pfützner, S. Steinhäuzer, Nucl. Phys. A **630**, 208c (1998).
12. K.-H. Schmidt, S. Steinhäuzer, C. Böckstiegel, A. Grewe, A. Heinz, A.R. Junghans, J. Benlliure, H.-G. Clerc, M. de Jong, J. Müller, M. Pfützner, B. Voss, Nucl. Phys. A **665**, 221 (2000).
13. A. Karnik, S. Kailas, A. Chatterjee, P. Singh, A. Navin, D.C. Bisaws, D.M. Nadkarni, A. Shrivastava , S.S. Kapoor, Z. Phy. A **351**, 195 (1995).
14. D.J. Hinde, M. Dasgupta, *Proceedings of the Tours Symposium on Nuclear Physics III, Tours, France, (1997)* (AIP Publishing, Tours, 1997).
15. N. Majumdar, T. Sinha, P. Bhattacharya, D.C. Biswas, L.M. Pant, R.K. Choudhury, D.M. Nadkarni, A. Saxena, R.G. Thomas. R.K. Choudhury, D.M. Nadkarni, *Proceedings of DAE Symposium on Nuclear Physics, Mumbai, India*, Vol. **41B** (1998) p. 226.

16. T. Murakami, C.-C. Sahm, R. Vandenbosch, D.D. Leach, A. Ray, M.J. Murphy, Phys. Rev. C **34**, 1353 (1986).
17. A.M. Samant, S. Kailas, A. Chatterjee, A. Shrivastava, A. Navin, P. Singh, Eur. Phys. J. A **7**, 59 (2000).
18. D.J. Hinde, A.C. Berriman, M. Dasgupta, J.R. Leigh, J.C. Mein, C.R. Morton, J.O. Newton, Phys. Rev. C **60**, 054602 (1999).
19. S.R.S. Murthy, *Proceedings of DAE Symposium on Nuclear Physics, Bombay, India*, Vol. **30A** (1987) p. 348.
20. R.K. Choudhury, D.M. Nadkarni, V.S. Ambekar, B.V. Dinesh, A. Saxena, M.S. Samant, D.C. Biswas, L.M. Pant, Pramana, **44**, 177 (1995).
21. E. Wiessenberger, P. Geltenbort, A. Oed, F. Gonnenwein, H. Faust, Nucl. Instrum. Methods Phys. A **248**, 506 (1986).
22. A. Saxena, A. Chatterjee, R.K. Choudhury, S.S. Kapoor, D.M. Nadkarni, Phys. Rev. C **49**, 932 (1994).
23. D. Hilscher, H. Rossner, Ann. Phys. (Paris) **17**, 471 (1992).
24. D.J. Hinde, H. Ogata, M. Tanaka, T. Shimoda, N. Takahashi, A. Sinohara, S. Wakamatsu, K. Katori, H. Okamura, Phys. Rev. C **39**, 2268 (1989).
25. M.G. Itkis, Yu. Ts. Oganessian, G.G. Chubarian, V.S. Salamatin, A. Ya. Rusanov, V.N. Okolovich, *Proceedings of the XV EPS Conference on Low Energy Nuclear Dynamics (LEND-95), St. Petersburg, Russia, 1995*, edited by Yu. Ts. Oganessian (World Scientific, Singapore, 1995) p. 177.
26. R.K. Choudhury, A. Saxena, A. Chatterjee, D.V. Shetty, S.S. Kapoor, M. Cinausero, L. Corradi, E. Farnea, E. Fioretto, A. Gadea, D. Napoli, G. Prete, A.M. Stefanani, D. Bazzaco, S. Beghini, D. Fabris, G. Montagnoli, G. Nebbia, C. Rossi-Alvarez, F. Scarlassara, C. Ur, G. Viesti, Phys. Rev. C **60**, 054609 (1999).
27. J. Terrell, Phys. Rev. **127**, 880 (1962).
28. A.Ya. Rusanov, M.G. Itkis, V.N. Okolovich, Phys. At. Nucl. **60**, 683 (1997).
29. U. Brosa, S. Grossmann, A. Müller, Phys. Rep. **197**, 167 (1990).
30. J. Blocki, J. Randrup, W.J. Swiatecki, C.F. Tsang, Ann. Phys. (N.Y.) **105**, 427 (1977).
31. R.W. Hasse, W.D. Myers, *Geometrical Relationships of Macroscopic Nuclear Physics* (Springer-Verlag, 1988).
32. A.J. Sierk, Phys. Rev. C **33**, 2039 (1986).